Supplementary Information

Two orders of magnitude boost in the detection limit of droplet-based micro-magnetofluidics with planar Hall Effect sensors

Julian Schütt[1,*], Rico Illing[1], Oleksii Volkov[1], Tobias Kosub[1], Pablo Nicolás Granell[1,2,3], Hariharan Nhalil[4], Jürgen Fassbender[1], Lior Klein[4], Asaf Grosz[5] and Denys Makarov[1,*]

[1]Dresden-Rossendorf e.V., Institute of Ion Beam Physics and Materials Research, Bautzner Landstrasse 400, 01328 Dresden, Germany

[2]Escuela de Ciencia y Tecnología, UNSAM, Campus Miguelete, B1650KNA San Martín, Buenos Aires, Argentina

[3]Instituto Nacional de Tecnología Industrial, Av. Gral Paz 5445, B1650KNA San Martín, Buenos Aires, Argentina

[4]Department of Physics & Institute of Nanotechnology and Advanced Materials, Bar-Ilan University, Ramat Gan 5290002, Israel

[5]Department of Electrical and Computer Engineering, Ben-Gurion University of the Negev, Israel

Keywords: Droplet microfluidics, planar Hall Effect, sensorics, contactless sensing, ferrofluids

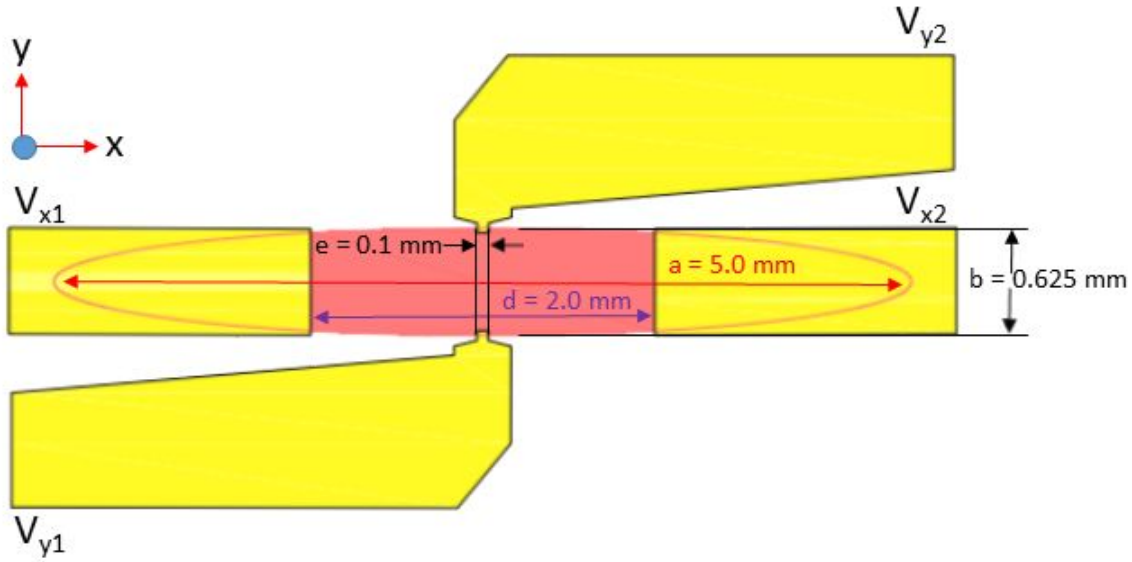

Figure S1: Schematic of sensor geometry. a and b are the long and short axes of the ellipse. The yellow regions are the gold electrical contact pads. The dimensions of the sensor and the electrical contacts are also noted.

Figure S2 shows planar Hall resistance measured across the sensor by passing a current (80 mA) along the long axis of the ellipse. Here, α is the angle between the applied field (H) and the long axis of the ellipse. At each angle α, the planar Hall resistance is measured with a saturating field (100 Oe) ON and OFF. When the field is ON (red filled circles), the planar Hall resistance exhibits sin2α indicating that the magnetization is fully aligned with the saturating field. When the field is switched OFF (blue filled circles) the planar Hall resistance is consistent with the magnetization being parallel to the long axis of the ellipse. Applying small magnetic fields at different angles relative to the long axis of the ellipse shows linear behavior of the planar Hall resistance vs H_{per} and from the slope of the graph (figure not shown) we extract a magnetic anisotropy field of ~ 9.5 Oe parallel to the long axis of the ellipse.[1]

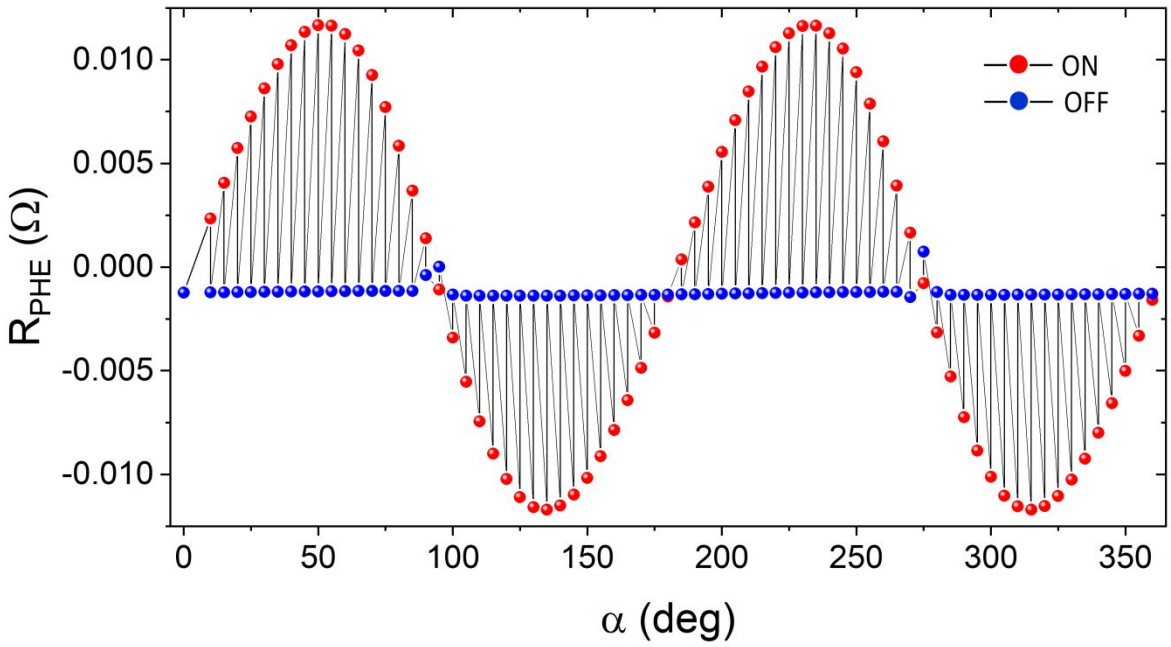

Figure S2: PHE resistance measured as a function of the angle α between an applied magnetic field (100 Oe) and the long axis of the ellipse. Black and red filled circles are measurements with the field on and after the field is switched off at each angle, respectively.

The amplitude spectral density of the sensor noise is measured in a bandwidth of 0.01 to 50 Hz. The sensor is excited with an ac current generated by a function generator (PXI-5421, National Instruments). Here, the sensor signal is modulated to a high frequency and amplified using a transformer matched amplifier.[1] The amplified output signal is sampled (PXI-4464, National Instruments) and demodulated using a digital synchronous detector. The output signal is filtered to a bandwidth of 100 Hz by a digital low pass filter. Details of the noise measurement setup and electronics can be found elsewhere.[1,2] All measurements are performed in a 3 layer magnetic shield (made of Amumetal) at room temperature. The sensor equivalent magnetic noise (B_{eq}) is determined by its input referred noise and its sensitivity.

A plot of the PHE sensor equivalent magnetic noise vs frequency is presented in Figure S3. In this, the red curve represents a fit according to

$$B_{eq} = A_0 + A_1.\frac{1}{f^{\gamma}}$$

where, A_0, A_1 and γ are fit parameters. The extracted values of the equivalent magnetic noise at 0.1 Hz, 1 Hz and 10 Hz are 249, 207 and 195 pT/√Hz, respectively, using A_0 = 271, A_1 = 206 and γ = 0.71.

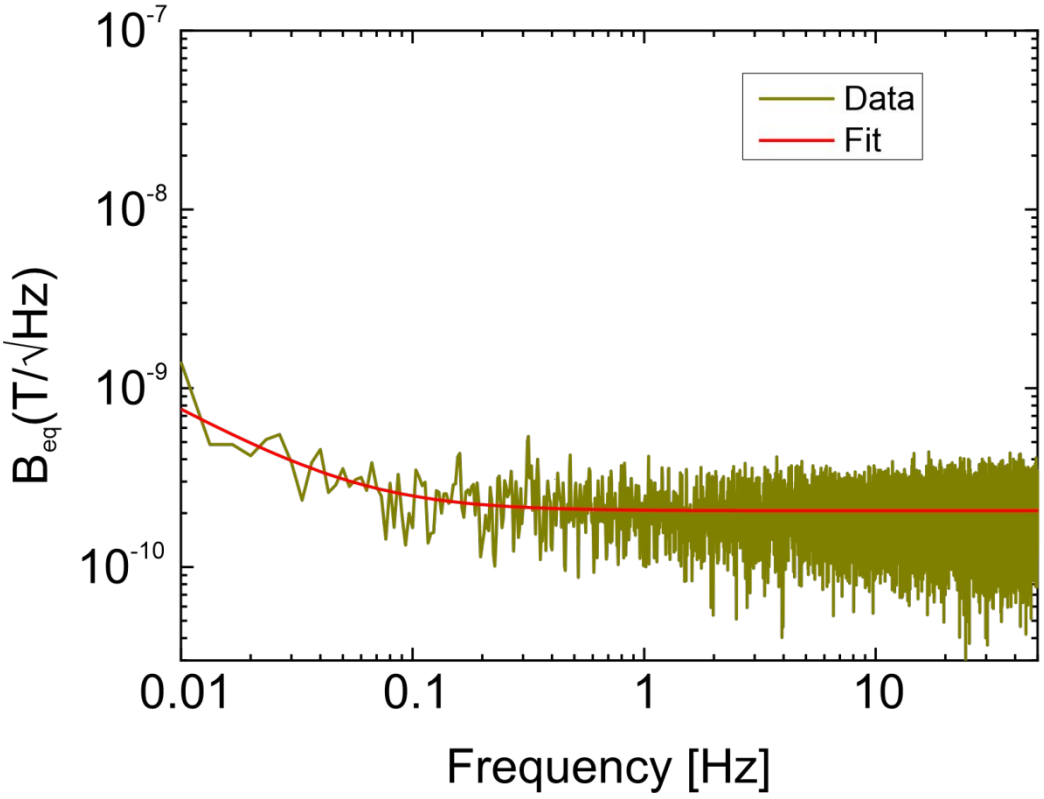

Figure S3: Equivalent magnetic noise (B_{eq}) vs frequency plot of a PHE sensor in a bandwidth of 0.01-50 Hz. The red curve is the fit according to the expression given in the text.

Whole experimental data for magnetic field gradient

Figure S4 summarizes the complete experimental data set of a real-time measurement exploring the dependency of the sensor response to magnetic fields. In this example, the mass of magnetic nanoparticles was set to 5 µg for each droplet. The droplets were continuously formed in the microtubes and guided over the sensor which was placed between the Helmholtz coils. Following, the amplitude of the external magnetic field was gradually decreased from 5 mT to "0 mT" (geomagnetic field) with a time step of around 2 min for each amplitude while the transverse resistance R_{xy} was recorded. As expected, for the highest magnetic field amplitude (5 mT) the current modulation was found at its maximum value (Figure S4, left side) and is gradually decreased with decreasing the field amplitude. Current peaks between the alterations of the field strengths are due to the alignment to the new magnetic field amplitude of the Helmholtz coils.

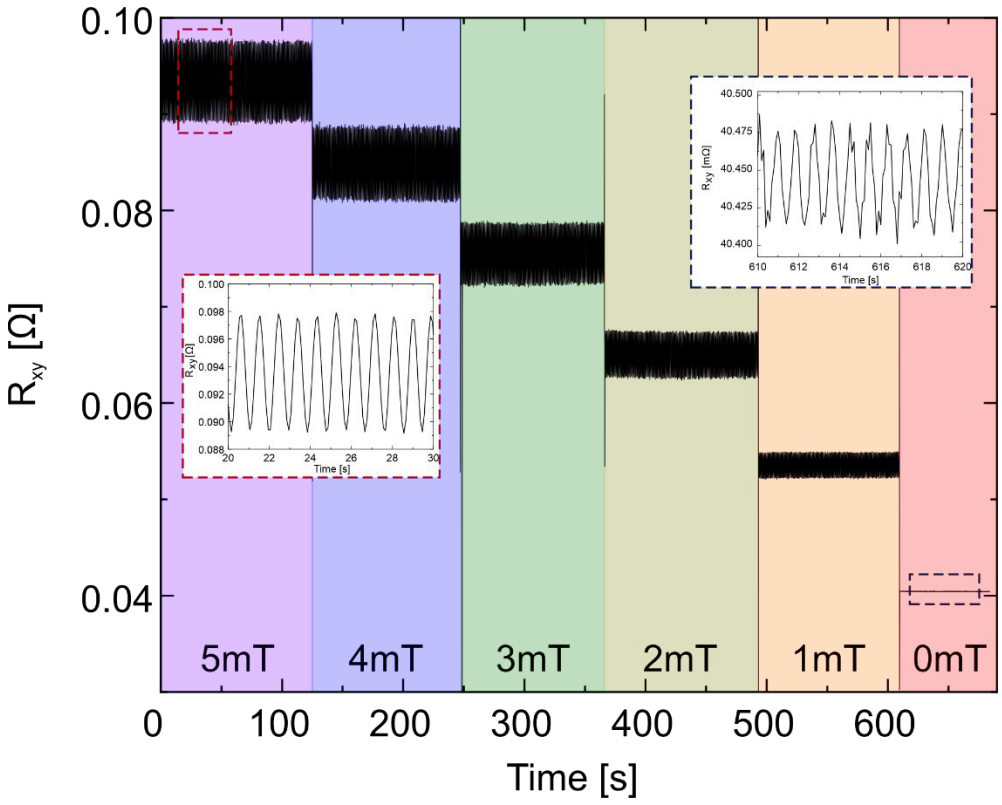

Figure S4: Whole data set of a measurement for exploration of the external magnetic field dependency. As expected, the higher the external magnetic field amplitude, generated by two Helmholtz coils, the more pronounced the droplet signal becomes.

Sensitivity of droplet magnetization in ferrofluid gradient

Figure S5 shows the full measurement of a series of ferrofluid droplets with a gradient of nanoparticle mass per droplet. For this, the ferrofluid phase was mixed prior to the separation into single droplets with DI water. The mixing was carried out in a Y-junction, which was connected to the microfluidic system prior to the T-junction. Creation of the gradient was achieved automatically using the software interface of the nemeSYS pump system. Both flow rates ferrofluid and DI water pumps were sinusoidal altered with a period of 3 minutes. Figure S7 shows a complete measurement from the smallest concentration (~1 mg(cm^3) to the maximum concentration (5 mg/cm^3) of ferrofluid and back to the initial concentration.

In addition, the numerical difference between the nanoparticle masses of 5 µg and 2.5 µg per droplet was found at ΔR = 32.36 µΩ (red dashed lines) resulting in a sensitivity of 12.94 µΩ/µg nanoparticle mass (See Inset). Further, the standard deviation of all droplets from the inset was found at $\sigma_{droplets}$ = 0.8 µΩ. Thus, the sensor's resolution is located at 124 ng or 0.12 mg/cm3 (2σ) and 247 ng or 0.24 mg/cm3 (4σ) nanoparticle mass per droplet in dynamic measurement. mode.

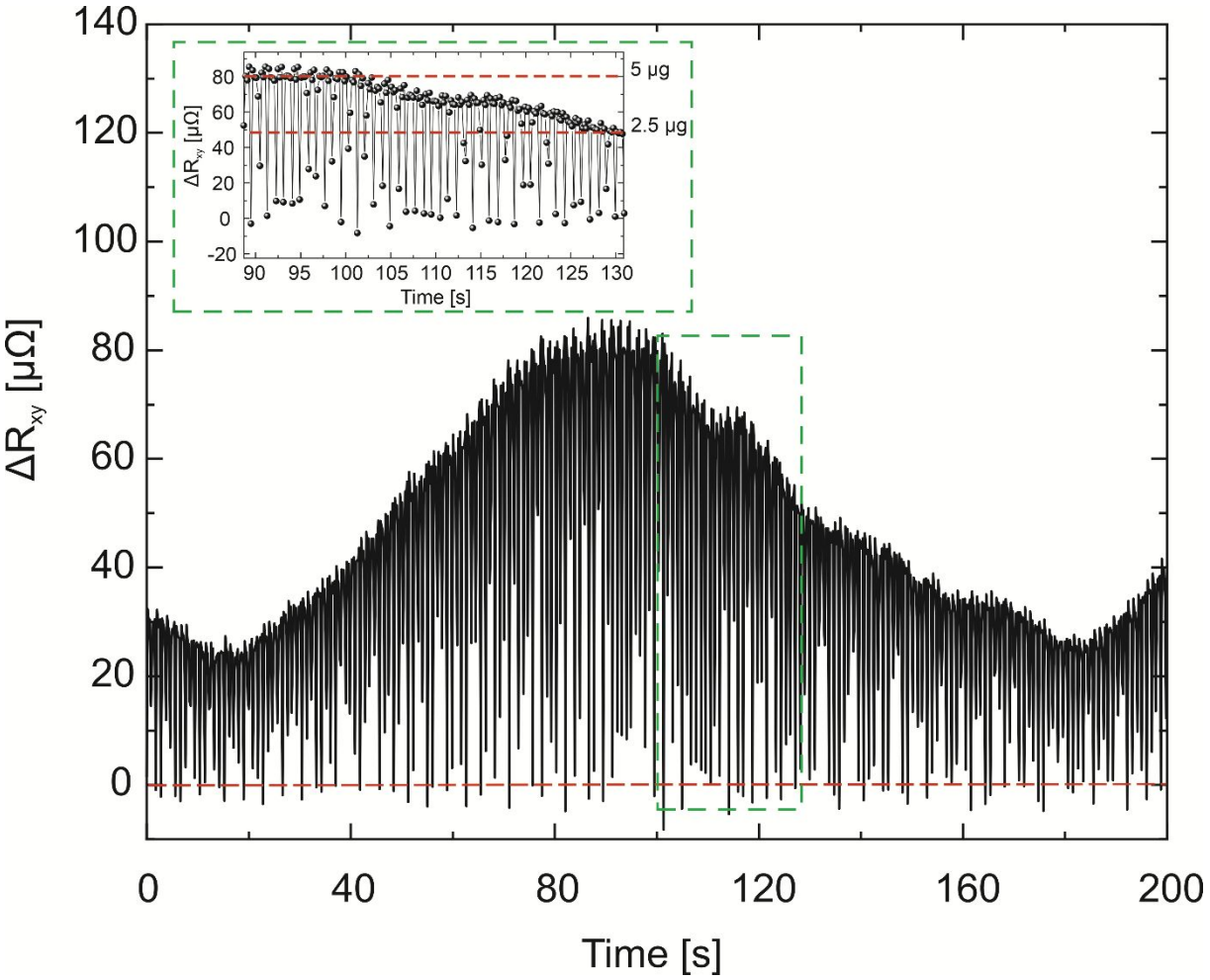

Figure S5: Ferrofluid gradient measurement. The ferrofluid stream was mixed with DI water prior to droplet formation by utilizing a Y-junction prior to the T-junction. The maximum concentration was set to 5µg of nanoparticle mass per droplet. A complete gradient measurement from the lowest to the highest concentration and back to the initial value can be seen.

Detection limit in geomagnetic field

Figure S6 demonstrates the detection limit of the magnetic content per droplet biased in the geomagnetic field. In this configuration, droplet signal in the time domain could be only observed until a magnetic content of 0.58 µg (main text, Figure 3). If the signal is transferred to the frequency domain using Fourier transformation, a clear peak could be observed at 1 Hz with the amplitude of approximately 4-5 µΩ (grey line). For smaller magnetic nanoparticle concentrations, no droplet signal could be observed in the time domain, but in the frequency domain, a peak of 2-3 µΩ could be observed with a mass of 0.4 µg per droplet (blue line).

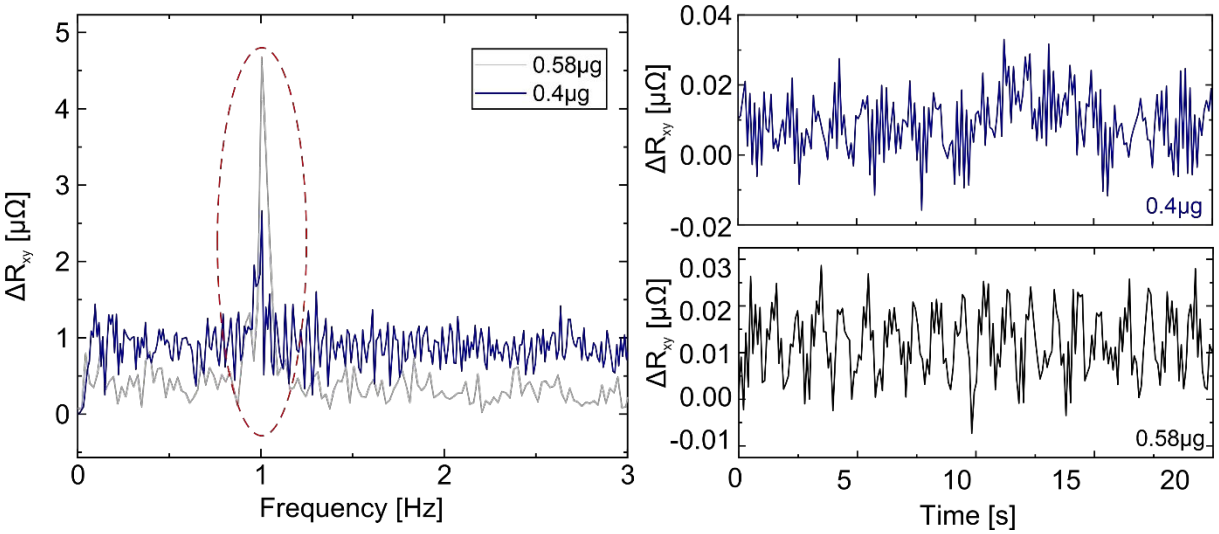

Figure S6: Detection limit of droplet, biased in geomagnetic field: Fourier transformation of the time dependent signal leads to a detection peak in the frequency domain down to 0.4 µg per droplet (blue line), which could not be observed in the time-domain (see right side).

Time-dependent droplet detection at various speeds in the geomagnetic field

In the following figure, the time-dependent signal of droplet detection using the PHE sensor can be seen. In the time-domain, droplets could be detected up to a frequency of approximately 2.2 Hz. Using Fourier transformation, droplets were detected up to the frequency of 13 Hz (main text, Figure 4A)

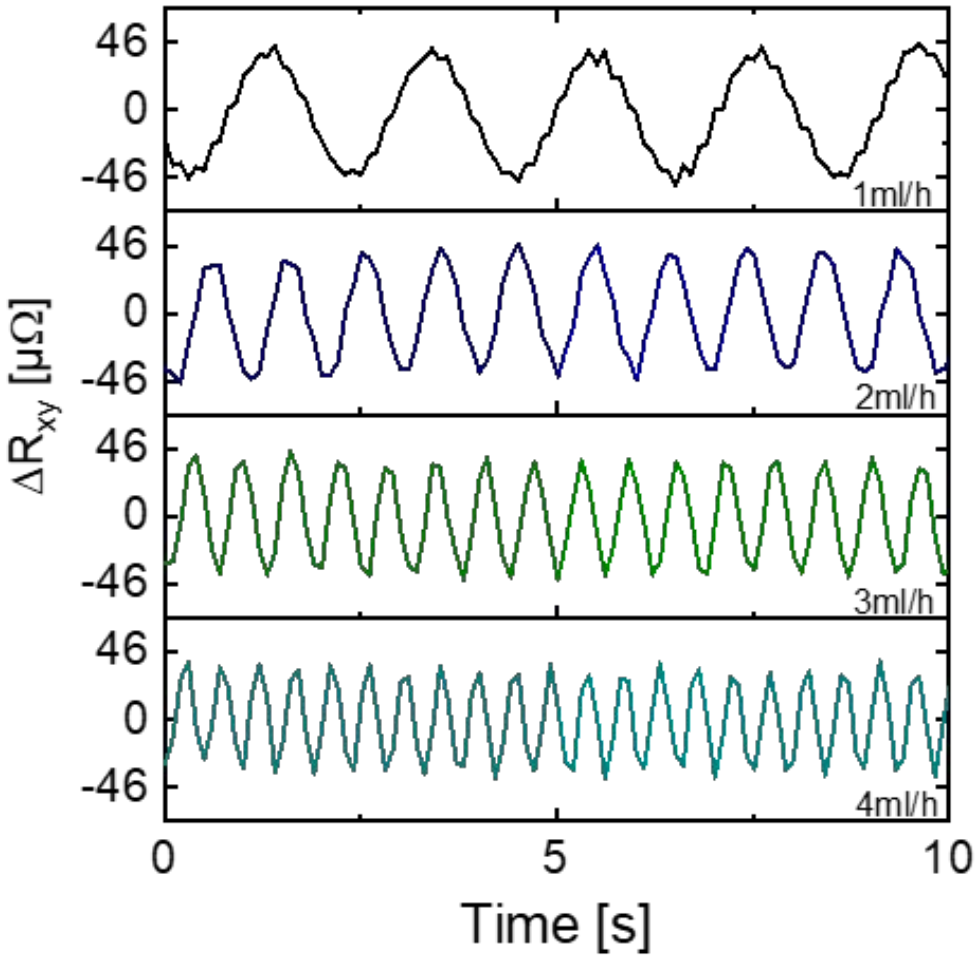

Figure S7: Droplet detection in the time-domain. The higher the flow rate, the higher is the droplet frequency. In this domain, droplets could be detected up to frequency of 2 Hz. For higher frequencies, Fourier transformation was utilized.

Supporting Video 1

Supporting Video 1 shows the microfluidic junction for droplet generation. In this connector, a T-junction is located in the middle, where the discontinuous phase (ferrofluid) is guided from the top and HFE oil as the continuous phase is guided from the left. This experimental design leads to a ferrofluid-in-oil emulsion, leaving the junction to the right. In this video, a flow ratio of HFE oil:ferrofluid of 2:1 was used, leading to droplet volumes of 70 nl. The flowrates were set to 2ml/h and 1ml/h for HFE oil and ferrofluid, respectively. The ferrofluid mass per droplet was set to 5mg/cm^3.

Supporting Video 2

Supporting Video 2 shows a close up of the experimental setup of the integration of microfluidics and PHE sensorics. Here, the ferrofluid droplet containing tubing was carefully aligned over the PHE sensor using a 3D-printed guidance geometry. In this video, the flow ratio was set to HFE oil:ferrofluid of 1:2, leading to droplet volumes of 250 nl, with a speed of 1 ml/h and 2 ml/h for HFE oil and ferrofluid, respectively. In this example, detection was carried out using ferrofluid droplets biased in the geomagnetic field with a ferrofluid mass per droplet of 5mg/cm^3.

References

1. A. Grosz, V. Mor, S. Amrusi, I. Faivinov, E. Paperno, and L. Klein. IEEE Sensors Journal, vol. 16, no. 9, pp. 3224–3230, 2016
2. A. Grosz, V. Mor, E. Paperno, S. Amrusi, I. Faivinov, M. Schultz, and L. Klein. IEEE Magnetics Letters, vol. 4, pp. 6 500 104–6 500 104, 2013